Canadian Science Publishing

ARTICLE

Potential for individual tree monitoring in ponderosa pine dominated forests using unmanned aerial system structure from motion point clouds[1]

Matthew B. Creasy, Wade T. Tinkham, Chad M. Hoffman, and Jody C. Vogeler

Abstract: Characterization of forest structure is important for management-related decision making, monitoring, and adaptive management. Increasingly, observations of forest structure are needed at both finer resolutions and across greater extents to support spatially explicit management planning. Unmanned aerial system (UAS) based photogrammetry provides an airborne method of forest structure data acquisition at a significantly lower cost and time commitment than existing methods such as airborne laser scanning (LiDAR). This study utilizes nearly 5000 stem-mapped trees in ponderosa pine (*Pinus ponderosa* Lawson & C. Lawson) dominated forests to evaluate several algorithms for detecting individual tree locations and characterizing crown area across tree sizes. Our results indicate that adaptive variable window detection methods with UAS-based canopy height models have greater tree detection rates compared with fixed window analysis across a range of tree sizes. Using the UAS approach, probability of detecting individual trees decreases from 97% for dominant overstory to 67% for suppressed understory trees. Additionally, crown radii were correctly determined within 0.5 m for approximately two-thirds of sampled trees. These findings highlight the potential for UAS photogrammetry to characterize forest structure through the detection of trees and tree groups in open-canopy ponderosa pine forests. Further work should investigate how these methods transfer to more diverse species compositions and forest structures.

Key words: detection, canopy height model, crown delineation, drone, forest structure.

Résumé : Il est important de caractériser la structure forestière pour éclairer les décisions de gestion, le suivi et la gestion adaptative. De plus en plus, des observations de la structure forestière sont nécessaires, tant à des résolutions plus fines que sur de plus vastes étendues, pour soutenir une planification de gestion spatialement explicite. La photogrammétrie basée sur des systèmes aériens sans pilote (SASP) fournit une méthode aéroportée d'acquisition de données sur la structure forestière à un coût et un investissement en temps nettement inférieurs à ceux des méthodes existantes telles que le balayage laser aéroporté. Cette étude utilise près de 5 000 tiges d'arbre cartographiées, dans des forêts dominées par le pin ponderosa (*Pinus ponderosa* Lawson & C. Lawson), pour évaluer plusieurs algorithmes de détection de l'emplacement des arbres individuels et de caractérisation de la surface de la couronne des arbres de différentes tailles. Nos résultats indiquent que les méthodes adaptatives de détection à fenêtre variable avec des modèles de hauteur du couvert forestier sur la base des données de SASP ont des taux de détection d'arbres plus élevés que l'analyse à fenêtre fixe pour un assortiment de tailles d'arbres. Avec l'utilisation des SASP, la probabilité de détecter des arbres individuels passe de 97 % pour l'étage dominant à 67 % pour les arbres opprimés du sous-étage. De plus, les rayons de la couronne ont été correctement déterminés, à moins de 0,5 m, pour environ les deux tiers des arbres échantillonnés. Ces résultats mettent en évidence le potentiel de la photogrammétrie basée sur les SASP pour caractériser la structure forestière grâce à la détection d'arbres et de groupes d'arbres dans les forêts de pins ponderosa dont le couvert n'est pas fermé. Des travaux supplémentaires devraient étudier comment ces méthodes peuvent s'appliquer à des compositions d'espèces et des structures forestières plus diverses. [Traduit par la Rédaction]

Mots-clés : détection, modèle de hauteur du couvert forestier, délimitation des couronnes, drone, structure forestière.

Introduction

Since the early 2000s, ecological management of dry, lower montane forest systems has increasingly focused on variability and spatial arrangement of horizontal and vertical forest structure (Lydersen et al. 2013). This emphasis has grown alongside the body of literature supporting connections between forest resilience to disturbance and the level of variation in forest structure (Larson et al. 2012). Silvicultural systems manipulating the horizontal and vertical forest structure in ponderosa pine (*Pinus ponderosa* Lawson & C. Lawson) have cascading effects on stand development pathways, disturbance regimes, and ecosystem services (Ziegler et al. 2017*a*). The creation of appropriately sized gaps and variable size tree groupings directly affects seedling establishment and competition-based tree mortality (Lydersen

Received 30 September 2020. Accepted 13 January 2021.

M.B. Creasy, W.T. Tinkham, and C.M. Hoffman. Department of Forest and Rangeland Stewardship, Colorado State University, Fort Collins, CO 80524-1472, USA.

J.C. Vogeler. Natural Resource Ecology Laboratory, Colorado State University, Fort Collins, CO 80523-1499, USA.

Corresponding author: Wade T. Tinkham (email: Wade.Tinkham@colostate.edu).

[1]This article is part of the special issue "Advances in forest mensuration and biometrics, featuring papers presented at the 2020 Western Mensurationists Conference".

et al. 2013). Retention of specific forest structures during treatment can fulfill multiple land use objectives, including providing wildlife habitat (Vogeler et al. 2016), stimulating understory plant responses (Cannon et al. 2019), and promoting pollinator communities (Rhoades et al. 2018). Silvicultural prescriptions promoting appropriately sized snag retention can provide nesting resources for woodpeckers, which are considered keystone species (Martin et al. 2004) and are often of management and conservation interest. The emphasis of forest restoration to balance ecosystem services with resilience to disturbance has led many land managers toward treatment strategies that enhance variation in forest structure (Churchill and Larson 2013; Tinkham et al. 2017). Although managers have shown a desire to implement spatially informed silvicultural prescriptions that create variability, most monitoring tools available to them were not developed with spatial management objectives in mind.

Fixed- and variable-radius plots have historically been the precedent for quantifying forest structure and have effectively informed land managers of stand-level averages; however, small distributed plots (i.e., ≤1/10th acre) assume forest homogeneity by focusing on average forest conditions (Dickinson et al. 2016). The limited spatial extent and data resolution of these plots comes from data collection protocols not designed for characterizing tree group variation and spatial arrangement that are critical in contemporary restoration approaches (Lutz 2015). Although these strategies provide important tree lists and even estimates of tree size distributions, they lack the extent or ability to describe spatial variability in forest structure necessary to inform silvicultural prescriptions. A complete enumeration of tree sizes and locations within a stand would provide the most useful data for restoration prescription development (Belmonte et al. 2020).

To better inform spatial objectives and characterize forest spatial variability, land managers have turned to novel data collection methods to characterize forest spatial variability (e.g., group sizes, openings, size distributions; Dickinson et al. 2016; Kane et al. 2019). Such methods are being called upon to provide comprehensive and accurate vertical forest structure data that can capture inter-tree relationships, variations in groups, and stand-level dynamics. This need for higher resolution and continuous spatial coverage of management units creates a unique methodological challenge. Synthesis of restoration efforts has pointed to incorporating remote sensing into forest monitoring as an effective strategy for supporting increased extents and frequencies of monitoring efforts (Belmonte et al. 2020).

The advent of airborne LiDAR (i.e., Light Detection and Ranging) provided new strategies to characterize horizontal and vertical forest structure heterogeneity across large extents (Wulder et al. 2012); these data have exhibited value for monitoring a suite of ecosystem services, including wildlife habitat (Vogeler and Cohen 2016), timber resources (Tinkham et al. 2012), and watershed health (Zurqani et al. 2020). Individual tree detection (ITD) methods provide useful approximations of individual tree locations, with LiDAR data capturing up to >90% of dominant overstory trees (Mielcarek et al. 2018), which is particularly true for conifer-dominated systems. The most commonly applied ITD methods operate by searching a canopy height model (CHM) with a moving window to identify local maximums characterized as treetops. Beyond the locations identified as treetops, LiDAR data provide precise tree height estimates and, when coupled with crown growing methods, can characterize crown area using a set of rules on a pixel-by-pixel basis within a CHM where ITD locations are often used as starting "seeds". Despite LiDAR's accurate estimation of forest structure, the technology's point density (1–30 points·m^{-2}) can limit the resolution of derived CHMs and potentially increases omission errors as clustered crowns fail to be distinguished, particularly in dense regeneration patches (Li et al. 2012). Additionally, the cost of airborne LiDAR limits repeated acquisitions for timely stand-level monitoring (Hummel et al. 2011), with financial efficiencies only reached for landscape monitoring (10s to 100s of thousands of hectares). The high cost of LiDAR for individual management projects and its limited success in describing variation in smaller tree size classes has opened the door for alternative methods of monitoring forest horizontal and vertical arrangement at fine spatiotemporal scales.

Unmanned aerial systems (UAS) have emerged as an alternative to airborne LiDAR for supporting local area management activities due to the low-cost of equipment (i.e., <$2000) that is capable of characterizing local wall-to-wall horizontal and vertical forest structure (Fraser and Congalton 2018; Mlambo et al. 2017). Most commonly, UAS are deployed with standard RGB cameras, which characterize three-dimensional forest structure through the application of structure from motion (SfM) photogrammetry algorithms (Maturbongs et al. 2019). Lower financial barriers to UAS platforms have incentivized exploration of these new approaches for improving temporal resolution in forest monitoring (Goodbody et al. 2017). Additionally, depending on camera and acquisition settings, UAS SfM can provide point densities much greater than airborne LiDAR (Iglhaut et al. 2019). The high density of UAS data could potentially enable accurate spatial characterization of individual trees within different canopy strata, improving enumeration of tree sizes and locations across relatively broad areas.

Many studies have evaluated ITD methods using LiDAR-derived CHMs, with an accuracy of 40%–90% depending on the forest type and structure (Heurich 2008; Maturbongs et al. 2019; Persson et al. 2002; Yu et al. 2011). Despite the variety of ITD methods, most use a fixed moving window to detect local maxima in a CHM, classifying these as trees (Popescu and Wynne 2004); however, the literature applying ITD methods to SfM-derived CHMs has been nominally investigated, with limited cross-comparison of ITD methods on higher data density UAS SfM-derived CHMs. Additionally, the choice of CHM crown growing methods starting from ITD "seed" locations has received limited attention.

The existing literature, especially regarding LiDAR, usually narrows the focus of ITD methods to include only overstory canopy due to the inherent difficulty of detecting trees with narrower, partially occluded crowns lower in the canopy (Heurich 2008; Panagiotidis et al. 2017). Additionally, ITD accuracy assessment is often challenged by having small validation datasets, data collected with consumer-grade GPS technology, and visual inspection of remotely acquired imagery. Limited validation makes it difficult to examine where ITD methods might break down in relation to forest structure and a tree's size compared with its neighbors. Recent studies have called for using large (>1 ha) stem-mapped sites for training and validation of remotely sensed forest observations (Chave et al. 2019). The use of large stem-mapped sites could allow for more comprehensive assessments of ITD methods across continuous observations of forest structure; such analysis can help to reveal any biases in the ability of ITD methods to represent forest structures.

In this study, we evaluate the transference of ITD methods developed for airborne LiDAR for use with high-resolution, fine-scale UAS SfM point clouds. Specifically, we use large continuous stem maps of ponderosa pine dominated forests to (1) examine the accuracy of individual tree detection methods and subsequent crown growing algorithms and (2) determine the effect of tree size and local forest structure on an individual tree's probability of detection.

Methods

Study area and validation data

We focused our investigation on the influence of forest structure on UAS tree detection within two ponderosa pine dominated study areas. Ponderosa pine is characterized by conical crowns resulting in a singular treetop, with stands comprised of a matrix of spatially aggregated tree clumps of a single cohort that are all similar in height (Ziegler et al. 2017*b*). The Lookout Canyon forest

Fig. 1. Relative locations shown on ESRI basemap in ArcMap (A) and example forest structures captured by UAS at MEF (B) and KNF (C). [Colour online.]

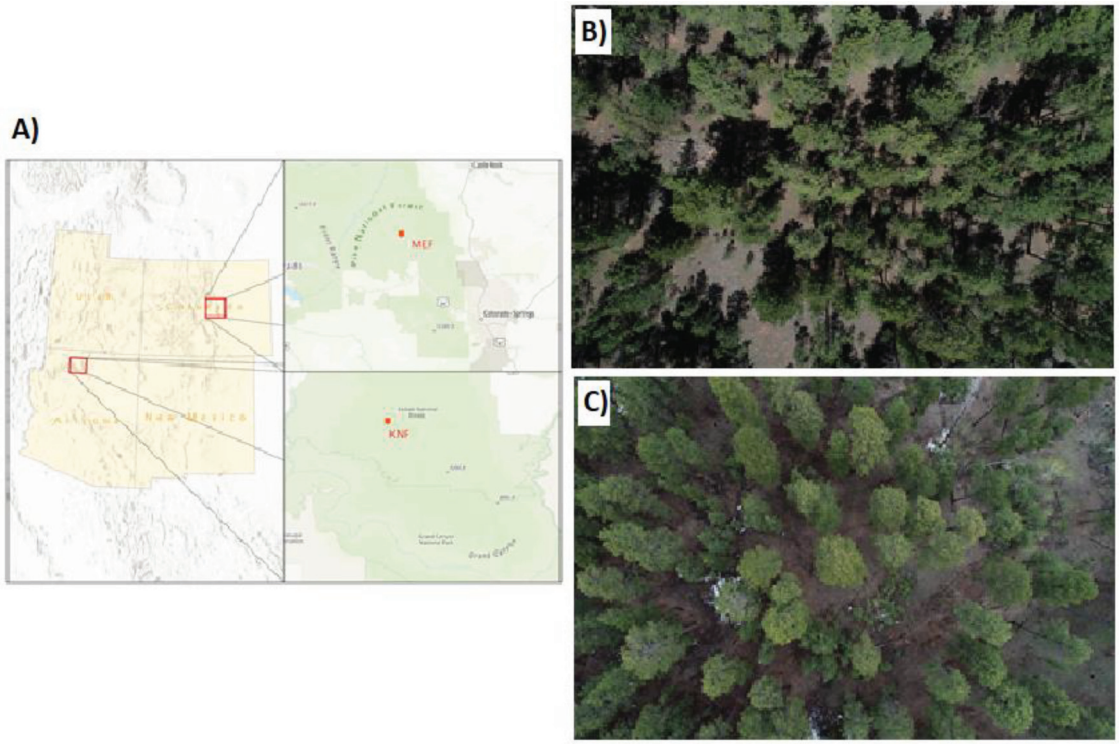

dynamics site on the Kaibab National Forest in Arizona is at an elevation of ~2400 m on the Kaibab Plateau, hereafter called KNF (Fig. 1). The site comprises two adjacent 4 ha treatments of pure ponderosa pine, including one control and one thinned in 1993 to 13.8 $m^2 \cdot ha^{-1}$ of basal area. Utilizing an existing grid of survey points, we stem-mapped the sites in May 2019, with observations of location, height, and diameter at breast height (DBH) recorded for all trees taller than 1.37 m. Survey locations within the site were established through a closed transect established by a total station with the site corners geolocated by a Trimble GeoXT using differential correction. The relative geolocation is estimated at 0.60 m, while the relative locations of trees are estimated at <0.10 m to each other. Current densities were 38.2 $m^2 \cdot ha^{-1}$ and 22.3 $m^2 \cdot ha^{-1}$ of basal area in the control and thinned sites, respectively, with local (5 m plot radius) height coefficients of variation of 42% and 35% for the two treatments. UAS data collection straddled the boundary of the two treatments at KNF to create a single study area.

Our second study area was the N1 forest dynamics site at the Manitou Experimental Forest on the Pike-San Isabel National Forest in Colorado, a square 9.3 ha site, hereafter called MEF. The MEF site is dominated by ponderosa pine with a minor ingrowth of Douglas-fir (*Pseudotsuga menziesii* (Mirb.) Franco) and blue spruce (*Picea pungens* Engelm.) with a sparse, grassy understory and a minor shrub component. The site's elevation averages ~2500 m, with a slope of ~5% to the southeast. In August 2018, all trees > 1.37 m in height had their location, height, and DBH recorded, revealing 25.9 $m^2 \cdot ha^{-1}$ of basal area and a local height coefficient of variation of 57%. Surveying was completed following the same protocols as the KNF site.

We randomly sampled tree crown diameters within the study sites to assess the accuracy of different crown growing methods. At each site, six randomly selected plots with a 15 m radius were used to sample trees. The longest crown axis and the perpendicular axis at 90° were measured for each selected tree to calculate the area of an ellipse, resulting in a total of 186 crowns: 97 at KNF and 89 at MEF.

UAS data collection and processing

All images were collected with a DJI Phantom 4 Pro quadcopter (Dá-Jiang Innovations Science and Technology Co. Ltd., Shenzhen, China) equipped with a 20-megapixel RGB camera at an 8.8 mm focal length. The aircraft recorded geolocation (*x*, *y*, and *z*) and camera parameter values for each captured photo to a manufacturer-stated vertical accuracy of ±0.5 m and horizontal accuracy of ±1.5 m (https://www.dji.com/phantom-4-pro; accessed 18 March 2019). Preprogrammed flight paths with a 90 m flight height, a flight speed of 5 $m \cdot s^{-1}$, and side and forward image overlap of 90% were set for MEF, while KNF was flown with a 100 m flight height, a flight speed of 4 $m \cdot s^{-1}$, and side and forward image overlap of 90%. All flights were conducted using the Altizure for IOS (Shenzhen, China) flight controller as it provides control of camera settings (in case of lighting changes), which were set to adjust automatically. Differences in flight parameterization between the sites ensured a constant ratio of flight height to vegetation height, while also ensuring that each acquisition could be completed with a single battery (~17 min). To comply with Part 107 of the United States Federal Aviation Administration regulations, the remote pilot in command and visual observer maintained a line of sight with the aircraft throughout each flight.

Point clouds were produced with Agisoft Metashape version 1.5.3 (www.agisoft.com; Agisoft LLC, St. Petersburg, Russia) through initial image feature identification, feature matching across photos, and location of images in three-dimensional space using the 431 and 476 UAS images as inputs from KNF and MEF, respectively. To ensure the most complete representation of tree crowns, combinations of the Metashape photo alignment "accuracy" and dense cloud build "quality" parameters were visually inspected for representation of overstory and understory trees. The settings used to develop the point cloud used for subsequent analysis (Table 1) provided sufficient resolution and limited filtering so that smaller understory trees were visually apparent. Metashape reported *xy* errors of 1.21 and 1.37 m for MEF and KNF, respectively. The resulting point clouds were processed in LAStools

Fig. 2. Final acquisition extent clipped to central area of interest at KNF (left) and MEF (right) with MCWS delineated crowns. [Colour online.]

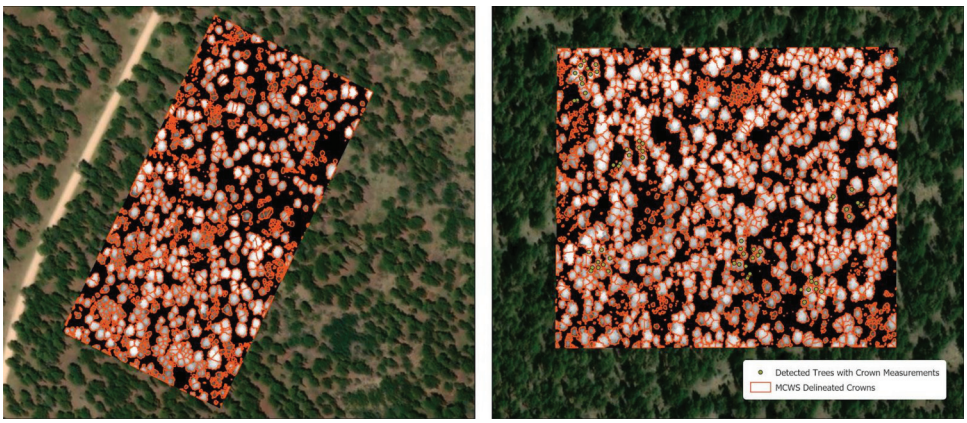

Table 1. Processing parameters for Agisoft Metashape SfM point cloud generation.

Parameter	Setting
Align photos	
Accuracy	Highest
Generic preselection	Yes
Reference preselection	Source
Reset current alignment	No
Key point limit	40 000
Tie Point Limit	4000
Apply masks to	None
Adaptive camera model fitting	Yes
Optimize alignment	
Adaptive camera model fitting	Yes
Build dense cloud	
Quality	High
Depth filtering	Mild
Calculate point colors	Yes
Calculate point confidence	No

version 1.2 (http://lastools.org) by identifying block minimum points every 0.25 m for spline fitting a digital terrain model. These point clouds were height normalized against the terrain models as elevation above ground and then converted to CHMs at 0.25 m resolution. At each site, the CHM was clipped to a single 4.5 ha area of interest (Fig. 2).

Individual tree detection

Processed CHMs were first searched using the fixed window and linear and exponential variable window functions to detect individual tree locations. This study evaluated seven fixed window parameterizations and 90 combinations of parameters for variable window local-maxima functions (Table 2) for a total of 97 ITD detections at each site. The fixed window function was tested at window sizes varying from 1 to 7 m in 1 m steps. The variable window function was tested using both linear (eq. 1) and exponential (eq. 2) functions that define the window radius as a function of height in the CHM.

$$\text{WR} = b_1 + Hb_2 \quad (1)$$

$$\text{WR} = b_1 \times e^{Hb_2} \quad (2)$$

where WR is the window radius (m), H is the height value (m) in the CHM, and the coefficients b_1 and b_2 were tested across a range of values. In the linear model (eq. 1), b_1 was tested from 0.3 to 0.6 with a 0.05 step and b_2 was tested from 0.05 to 0.09 with a 0.01 step. For the exponential model, b_1 was tested from 0.4 to 0.9 with a 0.05 step and b_2 was tested from 0.01 to 0.09 with a 0.01 step. Coefficient ranges were selected based on literature review and guidance from the ForestTools package (Plowright 2018), which was used to perform all tree detection in the R statistical programming language (R Core Team 2019).

Accuracy of tree detection and structure parameters

This study utilized 2270 and 2700 stem-mapped trees at the KNF and MEF sites to assess ITD method accuracy. Prior to evaluation of tree detection accuracy, the stem-mapped tree locations were overlaid on the final CHM and visually inspected. This inspection revealed no distortion within the CHM's representation of relative tree locations across the study extent. Following the methods of Silva et al. (2016), detected trees were matched with stem-mapped trees through a two-step process evaluating distance and height error between trees in each dataset. For a detected and stem-mapped tree to be considered a match, a maximum Euclidean distance (MED) and minimum height difference (MHD) must be met. This iterative process buffered one tree at a time according to the MED before checking the MHD. If multiple trees were found within the buffer, the tree with the smallest MHD was considered the match to the detected tree. After a match, both the detected and stem-mapped trees were removed before the next iterative match was identified. MED was set to 3 m to account for stem-mapping errors, georeferencing errors, and tree lean. The MHD was set to 10% of the field-inventoried height to account for observation errors in dense, mature forests (Andersen et al. 2006).

To assess detection accuracy across tree sizes, stem-mapped trees were classified into three strata based on their location within the distribution of heights at each study site (Fig. 3): overstory (>18 m at MEF; >20 m at KNF), intermediate (heights between upper and lower bounds), and understory (<6 m at MEF; <8 m at KNF). Trees were not assessed by any factors other than canopy strata as other demographic characteristics such as dead trees were minor components at both sites. The true positive (TP, correct detection), false positive (FP, commission error), and false negative (FN, omission error) detection rates were estimated at each site and by strata. The accuracy of these measurements was summarized to recall (r; eq. 3), precision (p; eq. 4), and F score (F; eq. 5) (Goutte and Gaussier 2005):

$$r = \frac{\text{TP}}{\text{TP} + \text{FN}} \quad (3)$$

$$p = \frac{\text{TP}}{\text{TP} + \text{FP}} \quad (4)$$

Table 2. Summary of individual tree detection and crown delineation functions and parameters used in this study.

Method	R package (function); citation	Variables
Individual tree detection		
Fixed window	ForestTools package (vwf); Popescu and Wynne (2004)	Window size (3×3, 5×5, 7×7 cells, etc.)
Variable window	ForestTools package (vwf); Popescu and Wynne (2004)	Window size (varies according to user-defined function in response to height)
Crown delineation		
Voronoi tessellation	lidR package; treetops from best vwf( ) models; Silva et al. 2016	Lmf (local maxima filter) Mac_cr_factor (maximum crown diameter given as a proportion of tree height)
Crown growing decision tree	lidR package; treetops from best vwf( ) models; Dalponte and Coomes, 2016	Lmf (local maxima filter) Th_tree (minimum tree height threshold) Th_seed (growing threshold 1) Th_cr (growing threshold 2) Max_cr (maximum crown diameter)
Watershed segmentation	lidR package; treetops from best vwf( ) models	Lmf (local maxima filter)

Fig. 3. Histogram of observed tree heights at KNF (left) and MEF (right) colored by canopy stratum. [Colour online.]

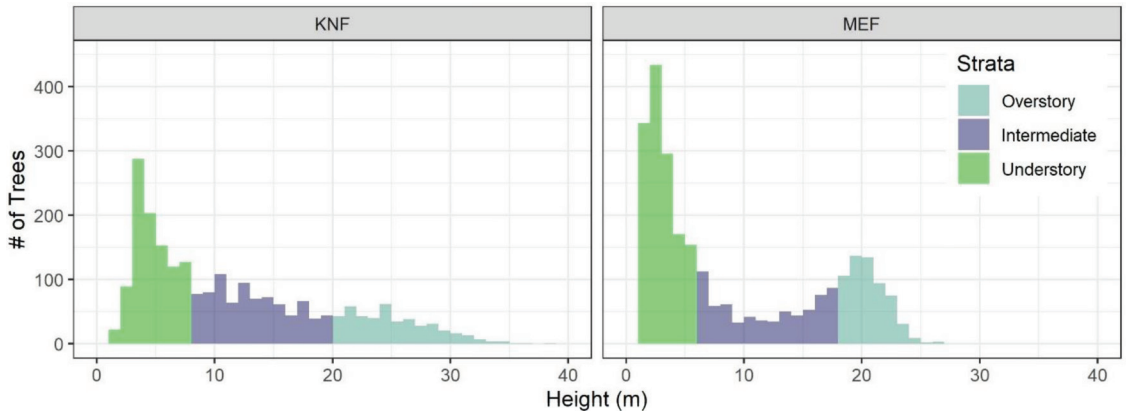

$$F = 2\frac{r \cdot p}{r + p} \quad (5)$$

Recall is the rate of tree detection, precision is a measure of detected tree correctness, and F score is overall accuracy of the method, which incorporates both precision and recall. The values of r, p, and F range from 0 to 1. If an ITD method has correctly identified trees according to its values of p and r, it will result in a higher F score. In the event of perfect segmentation, all values would be equal to 1. The best performing ITD methods ideally perform well across size groups, while minimizing omission and commission errors. Therefore, to establish the overall best performing equations for individual tree detection, overall F score was evaluated, and ties were broken through examining F scores for the overstory, intermediate, and understory strata. We identified the best overall performing exponential, linear, and fixed window models at both sites. Additionally, we compared matched stem-mapped trees with extracted heights to determine precision on a tree-by-tree basis. Errors were summarized using mean absolute error (MAE) and percentage root mean square error (%RMSE). Distributions of tree heights in each stratum were further compared using a two-sample Wilcoxon rank sum test.

Probability of tree detection

To understand how forest structure impacts ITD performance, we used logistic regression to determine the probability of a tree's detection based on the ITD method that maximized the F score. Separate models were fit for each tree size stratum where the response was classified as 1 for correctly matched trees and as 0 for omitted trees. Individual measures of a tree's height and DBH, along with local neighborhood structural attributes, were used as predictive variables. Local structure was summarized for a 5 m radius plot centered on each tree (Table 3) for trees per hectare (TPH), basal area ($m^2 \cdot ha^{-1}$), nearest-neighbor distance (metres; NND), and height percentile (%) calculated as tree height divided by tallest neighboring tree height × 100. Parameters were tested for collinearity using Pearson's correlation coefficient, with colinear variables removed when $r \geq 0.6$. The best subset of remaining variables was identified through stepwise forward–backward variable selection using the Akaike information criterion (AIC), where the best model subset was the one that minimized AIC. We performed logistic regression using the glm and regsubsets functions in the stats (R Core Team 2019) and leaps (Lumley 2020) packages of the R statistical programming language.

Crown growing

Most crown growing methods use detected treetops as "seeds" and evaluate surrounding CHM values to delineate the crown. After the top performing ITD method was determined by the overall F score, these "seed" tree locations were used as starting points for delineating crown areas. All crown growing was run in the R statistical program using the Dalponte, Silva, and watershed functions from the lidR package (Romain 2020) and the marker-controlled watershed function from the ForestTools package (Plowright 2018). The Dalponte2016() function uses a decision tree to grow crowns using ITD locations as seeds. Crowns are grown by iteratively adding surrounding cells if their height value is less than a defined

Table 3. Summary of tree and neighborhood structural attributes at the two study sites, presented as mean (standard deviation) of individual tree parameters or from 5 m radius local plots.

Study site	Stratum	Height (m)	DBH (cm)	Crown area (m^2)	NND (m)	Height percentile (%)	Basal area (m^2 ha^{-1})	TPH
KNF (N = 2270)	Overstory (n = 446)	25.2 (3.5)	54.5 (12.6)	163.8 (81.4)	2.47 (1.25)	97 (6)	64.4 (30.3)	462 (345)
	Intermediate (n = 820)	13.2 (3.3)	23.9 (8.9)	51.1 (39.1)	1.66 (1.04)	74 (21)	45.3 (27.5)	1,075 (747)
	Understory (n = 1004)	4.8 (1.6)	8.7 (4.2)	15.6 (8)	1.22 (0.99)	51 (28)	22.6 (20.2)	1,508 (1,163)
MEF (N = 2700)	Overstory (n = 592)	20.6 (1.6)	40.7 (8.1)	99.0 (60.9)	2.50 (1.17)	97 (5)	43.9 (16.4)	527 (261)
	Intermediate (n = 689)	11.9 (4.0)	22.6 (10.0)	58.6 (33.9)	1.87 (1.16)	76 (22)	30.4 (20.8)	852 (639)
	Understory (n = 1419)	3.0 (1.3)	4.4 (3.6)	15.5 (13.8)	1.44 (0.98)	39 (28)	12.8 (13.9)	1,293 (752)

Note: DBH, diameter at breast height; NND, nearest-neighbor distance; TPH, trees per hectare; MEF, Manitou Experimental Forest; KNF, Kaibab National Forest.

Table 4. Summary of best linear, exponential, and fixed window ITD models for both Manitou Experimental Forest (MEF) and Kaibab National Forest (KNF).

Rank	Model	Stratum	F score	Precision	Recall	True positive	False negative	False positive	No. of true trees	No. of detected trees	Height mean error (m)	Height RMSE (m)	Height RMSE (%)
Manitou Experimental Forest													
1	Linear function	Overall	0.58	0.71	0.49	0.49	0.51	0.20	2700	1854	0.10	0.62	11.8
	$WR = 0.4 + H \times 0.085$	Overstory	0.75	0.72	0.77	0.77	0.23	0.29	592	630	0.45	0.75	3.7
		Intermediate	0.53	0.60	0.48	0.48	0.52	0.32	689	547	0.10	0.56	5.3
		Understory	0.50	0.78	0.37	0.37	0.63	0.11	1419	677	−0.20	0.53	17.8
19	Exponential function	Overall	0.57	0.72	0.47	0.47	0.53	0.18	2,700	1754	0.12	0.62	11.2
	$WR = 0.5 \times e^{H \times 0.06}$	Overstory	0.75	0.72	0.78	0.78	0.22	0.31	592	641	0.45	0.75	3.6
		Intermediate	0.52	0.60	0.47	0.47	0.53	0.32	689	542	0.12	0.56	5.2
		Understory	0.48	0.84	0.34	0.34	0.66	0.07	1419	571	−0.20	0.52	17.4
70	Fixed window	Overall	0.50	0.57	0.45	0.45	0.55	0.34	2,700	2121	0.13	0.64	9.6
	$WR = 1$	Overstory	0.64	0.50	0.86	0.86	0.14	0.85	592	1011	0.33	0.75	3.7
		Intermediate	0.49	0.49	0.49	0.49	0.51	0.52	689	700	0.16	0.59	4.9
		Understory	0.39	0.88	0.25	0.25	0.75	0.04	1419	410	−0.18	0.49	16.4
Kaibab National Forest													
1	Linear function	Overall	0.57	0.65	0.51	0.51	0.49	0.28	2270	1790	0.68	1.80	18.0
	$WR = 0.6 + H \times 0.065$	Overstory	0.71	0.70	0.72	0.72	0.28	0.31	446	459	1.63	2.43	10.0
		Intermediate	0.57	0.79	0.45	0.45	0.56	0.12	820	460	0.83	1.91	15.0
		Understory	0.51	0.55	0.47	0.47	0.53	0.39	1004	871	−0.08	1.07	23.5
11	Exponential function	Overall	0.57	0.67	0.49	0.49	0.51	0.24	2270	1667	0.70	1.81	17.3
	$WR = 0.4 \times e^{H \times 0.06}$	Overstory	0.70	0.70	0.71	0.71	0.29	0.31	446	454	1.62	2.42	10.0
		Intermediate	0.57	0.81	0.44	0.44	0.56	0.11	820	450	0.84	1.91	14.9
		Understory	0.50	0.58	0.44	0.44	0.56	0.32	1004	763	−0.08	1.06	22.5
63	Fixed window	Overall	0.52	0.64	0.44	0.44	0.56	0.25	2270	1560	0.89	1.84	14.7
	$WR = 1$	Overstory	0.60	0.49	0.78	0.78	0.22	0.81	446	713	1.40	2.34	9.6
		Intermediate	0.56	0.83	0.43	0.43	0.57	0.09	820	420	1.18	1.89	14.1
		Understory	0.42	0.70	0.30	0.30	0.70	0.13	1004	427	−0.03	0.87	19.4

Note: Models rank is based on all possible model parameterizations tested at each site. Accuracy results for all model parameterizations are presented in Supplemental Table S1.[2]

maximum difference from the seed's height, less than a maximum crown ratio, or a maximum crown diameter is reached (Dalponte and Coomes 2016). The Silva et al. (2016) function starts with a buffer around each ITD tree point and separates the crowns using the centroidal Voronoi tessellation (Silva et al. 2016). Values within a resulting tree crown below a user-defined percentage of the tree's height are then removed from the crown region. Lastly, the watershed() function of the lidR package uses an inverted watershed segmentation method. Watershed-based ITD functions can either use input tree locations using a "marker-controlled" approach or find local maxima independently. The mcws() function (marker-controlled watershed) from the ForestTools package was also run. The user-defined parameters within each function are summarized in Table 2 and set to the default except where noted. The extracted tree crown area was compared with matched stem-mapped tree crown area to determine precision on a tree-by-tree basis. Errors were summarized using MAE and %RMSE. Crown radius of a circle was also back-calculated from field inventory and detected crown areas for further comparison.

Results

Observed forest structure

Both study sites exhibited complex vertical and horizontal forest structure with high levels of variation in the individual tree and local neighborhood structural attributes (Table 3). Trees at KNF tended to be ~20% taller in each canopy stratum than those at MEF, with the KNF overstory stratum having twice the variation within it. Across the site strata, the only substantial differences in the relative height of a tree compared with its neighbors was that understory trees at KNF tended to be taller in both relative and absolute terms than understory trees at MEF. Despite having larger trees, KNF tended to have trees arranged closer to neighboring trees across all strata. KNF's height distribution appears unimodal and skewed to the right, typical of a multiage or all-age forest structure

[2]Supplemental Table S1 is available with the article at https://doi.org/10.1139/cjfr-2020-0433.

Fig. 4. Violin plots of *F* scores for the three model forms across the four canopy strata. Inset box plots represent median and quartile values.

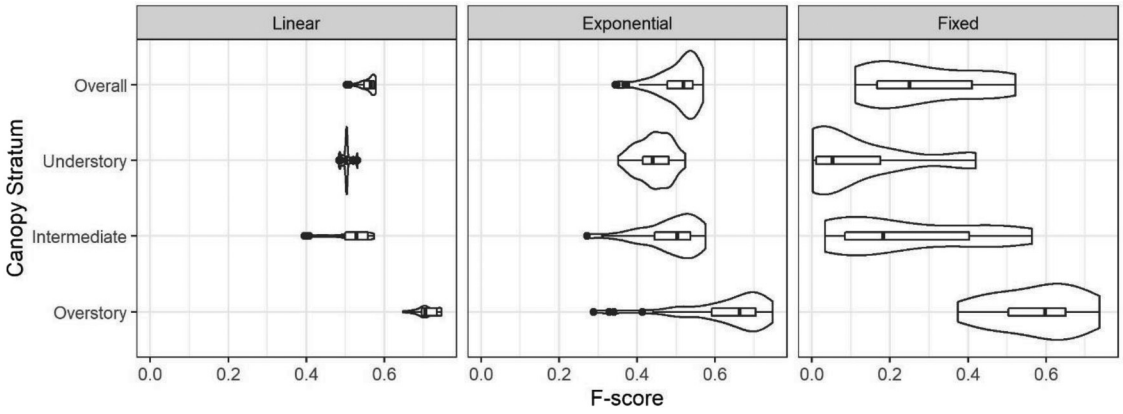

Fig. 5. Density distributions of tree heights at the two study sites with field-observed data outlined in blue and the top-ranked individual tree detection model values outlined in red. Overlapping segments of the distributions appear darker. [Colour online.]

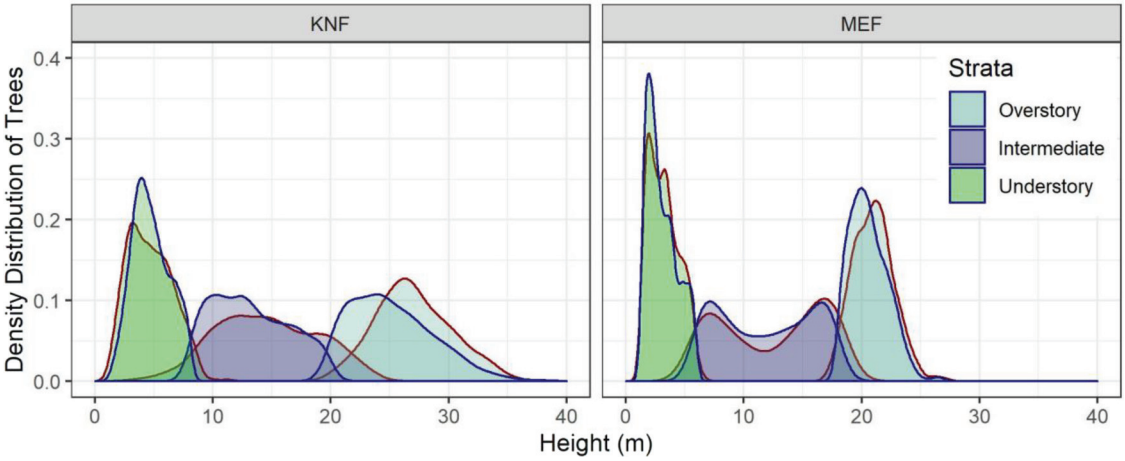

(Fig. 3). Conversely, the bimodal appearance of the MEF height distribution is more indicative of a two-age forest structure. Although the overall distributions of height differ slightly between the sites, both sites have large local (5 m radius) coefficients of variation in height at an average of 39% and 57% for KNF and MEF, respectively.

ITD model performance

Evaluation of the ITD process showed that linear models fit within the variable window function produced the 12 and 7 highest ranked models based on the overall *F* score at MEF and KNF, respectively (Table 4). The linear models also provided a narrower range and consistently higher *F* scores for each canopy stratum (Fig. 4). Additionally, each model form at the two respective sites had similar overall performance, although the best model parameters varied slightly. At both sites, exponential models performed similarly to the linear models, except that exponential models tended to have greater omission rates in the understory stratum. Consistently, 1 m was the best fixed window size, as determined by *F* score, but consistently performed substantially worse than both the linear and exponential variable window functions (Table 3). The linear model's performance was the least sensitive to parameter selection (Fig. 4), while the fixed window *F* scores fluctuated from a high of 0.74 to 0.0 in the different canopy strata.

The total number of overstory stratum trees detected (TP + FP) in the best models was over by 6.4% and 2.9% of the inventoried tree counts at MEF and KNF, respectively (Table 4); however, detection accuracy varied across the canopy strata. Errors shift to an underdetection of the total number of trees by 20.6% and 43.9% in the intermediate stratum and 59.8% and 13.2% in the understory stratum for MEF and KNF, respectively. Both the linear and exponential variable window functions provided similar mean height errors for each of the canopy strata, with the overall error being less than 0.70 m. This positive bias in extracted tree height tended to be two to six times larger at KNF than at MEF (Table 4). Height RMSE was 4%–10% in the overstory, increasing through the shorter canopy strata to 16%–24% in the understory.

Probability of tree detection

Visual comparison of height distributions for the stem-mapped trees and trees extracted with the best linear model follow similar trends (Fig. 5). The largest departure in the distributions occurred at the KNF study site, with overstory and intermediate extracted tree heights being slightly taller than the field-observed values. Extracted heights for all strata pairs are different except for the KNF understory ($P = 0.9856$) and MEF intermediate ($P = 0.3629$) strata, according to the Wilcoxon rank sum test.

Regression modeling indicates that the factors influencing the probability of detecting individual trees varied across canopy strata (Table 5). Regardless of strata, trees that were relatively taller than their local neighbors (height percentile) had a greater probability of

Table 5. Best model subset from logistic regression to predict the probability of extracting a tree given local forest structure in a 5 m radius of a tree, broken out by canopy stratum.

Parameter	Coefficient	SE	*Z* value	*P* value
Overstory stratum				
Intercept	−4.5404	1.2743	−3.563	<0.001
Height percentile	0.0659	0.0127	5.170	<0.001
Basal area (m^2 ha^{-1})	−0.0106	0.0029	−3.645	<0.001
Intermediate stratum				
Intercept	−0.8171	0.5939	−1.376	0.1689
Height percentile	0.0223	0.0069	3.215	0.0013
Basal area (m^2 ha^{-1})	−0.0668	0.0148	−4.504	<0.001
Height percentile : basal area (m^2 ha^{-1})	0.0005	0.0002	2.770	0.0056
Understory stratum				
Intercept	−1.1015	0.1346	−8.186	<0.001
Height percentile	0.0164	0.0018	9.323	<0.001
Basal area (m^2 ha^{-1})	−0.0176	0.0033	−5.302	<0.001
Distance to nearest neighbor (m)	0.1693	0.0407	4.161	<0.001

Fig. 6. Probability of detecting understory stratum trees based on a tree's height compared with neighbors within 5 m, nearest-neighbor distance (m; NND), and basal area per hectare estimated from a 5 m radius plot set to 0 m^2 ha^{-1} (left) and 20 m^2 ha^{-1} (right).

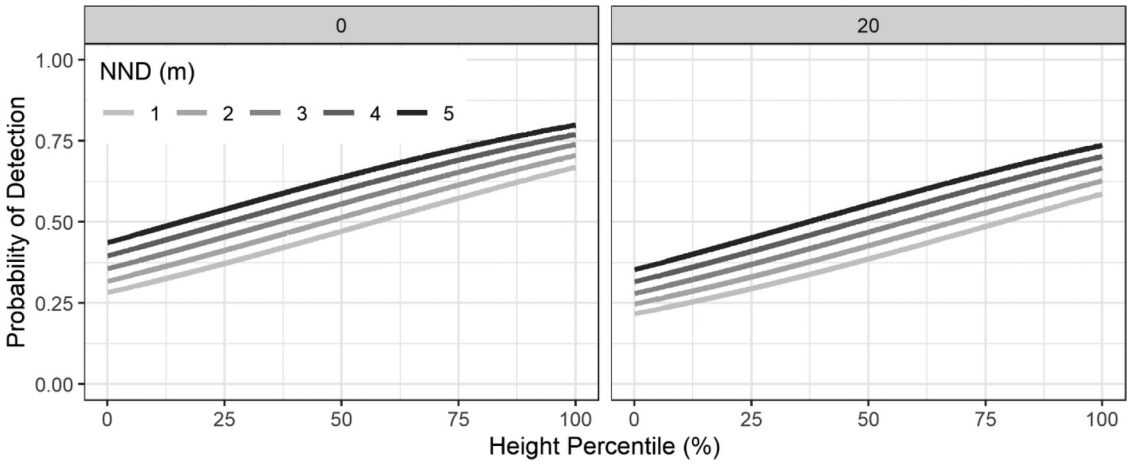

Fig. 7. Probability of detecting overstory stratum trees (left) and intermediate stratum trees (right), based on a tree's height compared with neighbors within 5 m and basal area per hectare estimated from a 5 m radius plot.

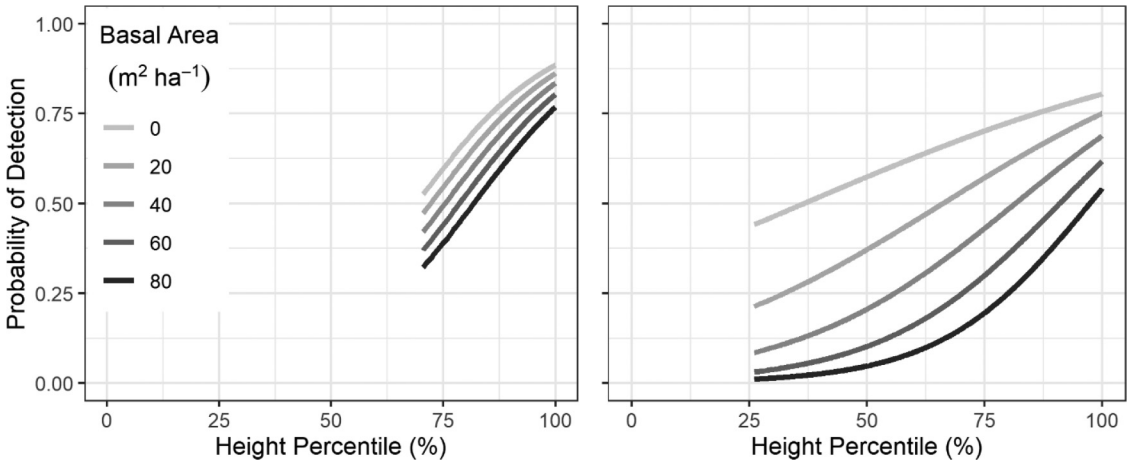

detection (Figs. 6 and 7). In the overstory and intermediate strata, the probability of detection was negatively related to basal area per hectare (Table 5). The influence of basal area for intermediate trees had a six times greater effect on reducing the probability of detection. This effect in the intermediate stratum also interacted with height percentile such that increasing stand density could reduce the probability of detection to 0% for trees less than half the height of a neighboring tree (Fig. 7).

The understory stratum shows similar dynamics (Fig. 6), except that increasing the distance to the nearest neighboring tree increases the probability of detecting understory trees (Table 5). For every metre of distance to the nearest neighbor, there is an almost 4% increase in the probability of detection, indicating that open-grown trees have a significantly greater likelihood of being detected (Fig. 6).

Crown growth

Individual tree crown growing methods were tested using correctly detected trees only. Of the tested crown growing methods, all but the lidR watershed method consistently underestimated the crown area (Table 6) using the tested UAS data acquisition and processing parameters. Overall, the lidR watershed method provided the smallest crown area bias at 3.68 and 1.40 m^2 at KNF and MEF, respectively. The lidR watershed method tended to overestimate small crowns and underestimate larger crowns (Fig. 8). Crown radius RMSE across all methods ranged from 0.76 to 0.82 m at KNF and from 0.55 to 0.65 m at MEF. The lidR watershed method was the best performing method, correctly extracting 41% of crown radii to within 0.25 m and 64% to within 0.50 m. The lidR watershed method also provided the best predictions of the total crown area, underestimating the total crown area by 24.8% at KNF and 13.3% at MEF (Table 6). Although some of the other evaluated methods performed similarly for an individual metric, none of these methods consistently minimized bias and precision as well as the lidR watershed method.

Discussion

Tree detection and crown growing performance

This study evaluated three individual tree detection algorithms with 97 different parameterizations at two study sites to identify the best strategy for detecting trees in complex uneven-aged ponderosa pine forest structures. The best performing parameterization, according to *F* score, provided overall tree detection accuracies of 78.8% at KNF and 68.7% at MEF. Standard ITD methods performed on LiDAR or SfM-derived CHM have detected real trees with accuracies ranging from 40% to 90% (Heurich 2008; Maturbongs et al. 2019; Persson et al. 2002). The wide range of tree matching success in the literature can be attributed to variation in forest structures, the methods tested, and the size of trees included for analysis, which typically target only overstory trees (Zhen et al. 2016). The overstory tree detection accuracy in this study was 97.2% and 93.9% at KNF and MEF, respectively, which exceeds expectations based on previous literature (e.g., Belmonte et al. 2020; Yu et al. 2011). The increased overstory detection accuracy is attributed to the variable window approach providing a range of search window sizes that better fit the crowns of trees ~10–30 m tall, as opposed to the more commonly applied fixed window approach that only applies a single window size.

The literature on individual tree detection has evolved to use *F* score as a more holistic measure of accuracy assessment as it integrates the TP, FP, and FN rates (Goutte and Gaussier 2005). Our best overall *F* scores were 0.57 and 0.58 at KNF and MEF, respectively. With improved detection of larger trees, the overstory *F* scores increase to 0.71 and 0.75 for KNF and MEF, respectively. By comparison, Mohan et al. (2017) matched detected trees with real trees through a visual assessment that identified 367 trees and resulted in an *F* score of 0.86, but only visually discernible trees from the imagery were included. More rigorously, Silva et al. (2016) achieved an *F* score of 0.83 by applying a similar tree-based matching logic used in this study but allowed trees to match within a 10 m distance to accommodate GPS errors and only tested forest densities up to 200 trees per hectare. The small reduction in *F* score in the present study is attributed the use of stem-mapped trees across a wide range of forest structures and rigorous tree-level matching to determine TP detections (i.e., 3 m horizontally and 10% of field height), resulting in stricter accuracy assessments than the aforementioned studies. Given that these studies evaluated the ability of fixed window detection to observe dominant tree structures, it is promising to see that the current study was able to provide similar results in the overstory while maintaining reasonable detection throughout all tree size strata.

Of the tested individual tree detection methods, linear models used in the variable window function provided the 18 highest

Table 6. Assessment of the ability of crown-growing methods to characterize individual tree crown area and radius for only extracted trees, as well as total extracted crown area error as a proportion of field-observed crown area (Manitou Experimental Forest (MEF) and Kaibab National Forest (KNF)).

	Crown delineation method	KNF	MEF
Crown area mean error (m^2)	lidR Watershed	3.68	1.40
	ForestTools MCWS	−4.79	−2.18
	lidR Dalponte	−7.30	−4.04
	lidR Silva	−7.48	−4.01
Crown area RMSE (m^2)	lidR Watershed	16.53	10.45
	ForestTools MCWS	16.16	8.46
	lidR Dalponte	15.85	9.58
	lidR Silva	16.03	9.74
Crown radius mean error (m)	lidR Watershed	0.21	0.09
	ForestTools MCWS	−0.32	−0.14
	lidR Dalponte	−0.44	−0.26
	lidR Silva	−0.43	−0.24
Crown radius RMSE (m)	lidR Watershed	0.76	0.65
	ForestTools MCWS	0.85	0.55
	lidR Dalponte	0.83	0.61
	lidR Silva	0.82	0.61
Total crown area error (%)	lidR Watershed	−24.8	−13.3
	ForestTools MCWS	−37.6	−35.0
	lidR Dalponte	−44.3	−41.6
	lidR Silva	−44.3	−42.2

Fig. 8. Observed versus lidR watershed extracted individual tree crown area. Dashed lines represent linear regression for each of the study sites; the solid line represents a one-to-one relationship for reference.

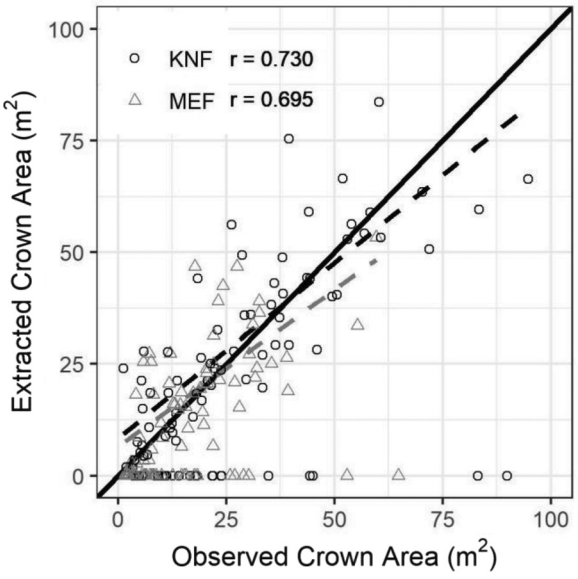

Fig. 9. Contour plot of *F* scores based on linear (left panels) and exponential (right panels) model coefficients, with higher *F* scores indicated by lighter colors. *F* scores have been averaged across the two study sites for each set of unique model coefficients and are arranged top to bottom as overall, overstory, intermediate, and understory strata. [Colour online.]

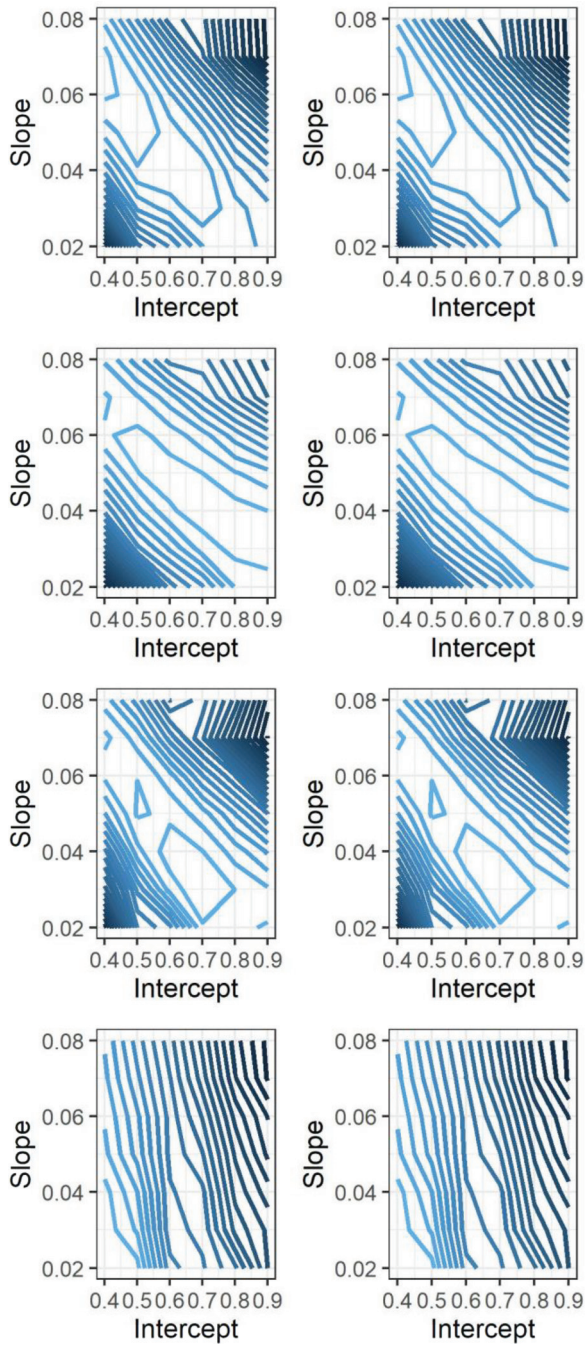

ranked outputs at MEF and 10 at KNF. Despite the consistently greater performance of the linear models, the best exponential models were similar in performance. The consistently high *F* scores found through the top 20 models at both sites implies some flexibility in ITD formula coefficients that improve overstory and intermediate strata detections (Fig. 9); however, when considering all trees > 1.37 m tall, the ITD formula coefficient space narrows for both the linear and exponential models to intercept values of <0.4 and slope or exponents around 0.07 (Fig. 9). This use of a small intercept term appears to allow for reasonable detection of smaller understory trees, and when used in combination with a relatively steep slope term, they can scale the search window to be large enough to not over-segment individual tree crowns in the overstory stratum. The optimal parameter search conducted in this study likely achieved higher accuracy estimates than might be expected if the parameters were applied to another ponderosa pine dominated site due to variations in tree size distributions and densities; however, the narrow range in *F* scores produced by the linear model (Fig. 4) suggests that this approach may have broader application within ponderosa pine forest systems. Application of these results to other ponderosa pine systems will require visual inspection of detected tree locations against the high-resolution orthophotographs provided by the UAS system to ensure that trees do not appear over- or under-segmented in their detection. Although our results indicate improved performance in tree detection from variable window functions compared with fixed windows, future studies should explore adaptive variable window functions such as piecewise regression to achieve more consistent accuracies across tree sizes. It is unclear how ITD conducted with variable window functions will perform in coniferous forest systems with greater species diversity or vertical heterogeneity, and further testing of these methods is needed across a range of ecosystems.

Crown area mean error varied widely across methods, with the lidR watershed method being the most accurate and producing a more natural crown representation (Fig. 10). The more natural crown shapes are attributed to the method's decision-making process on a pixel-by-pixel level. Comparatively, the lidr Silva and lidr Dalponte methods both utilize geometric processes to divide interlocking crowns that produce straight lines between trees.

This study's precision in extracted crown radii slightly improves on findings in Panagiotidis et al. (2017), who found a crown diameter RMSEs of 0.82 and 1.04 m for two study sites. Despite being in a conifer-dominated system, this difference is likely due to greater canopy cover and vertical forest structural variation in the area studied by Panagiotidis et al. (2017), both of which are known to occlude intermediate and understory trees, resulting in increased ITD and crown delineation errors. Average crown areas at KNF were much larger than crowns tested at MEF; therefore, the smaller pixel size may have helped to mitigate error that could have been present with a larger pixel size of ≥0.5 m. As crowns were grown in our study from detected tree *X* and *Y* coordinates, there are instances where field-measured trees were not correctly matched with detected trees. This error is restricted in calculating crown area and radii errors at the individual tree level but could explain the positive bias in our best performing method. Additionally, the total crown area was directly compared regardless of whether a tree was detected or not. This omission error propagated through to cause an underestimation of the total crown area across methods from −44.3% to −24.8% at KNF and −33.2% to −13.3% at MEF (Table 6).

Omission modeling

The best performing ITD methods closely matched the total number of trees in the overstory and intermediate strata (Table 4) with minimal errors in tree heights; however, distributions of tree heights only matched for the KNF understory and MEF intermediate strata, with the other canopy strata significantly differing from field values (Fig. 5). The large omission error for intermediate stratum trees at KNF is attributed to greater spatial aggregation of trees that can be seen through the increase local neighborhood basal areas compared with MEF (Table 3). Most of these omitted trees were in a dense group and at least 20% shorter than a neighbor (Fig. 7). The relatively high basal areas seen in this study are typical of untreated ponderosa pine forests (Tinkham et al. 2017) and indicate that UAS

Fig. 10. Visual representation of the four crown growing methods: (A) lidR watershed; (B) ForestTools marker-controlled watershed; (C) lidR Silva; and (D) lidR Dalponte. [Colour online.]

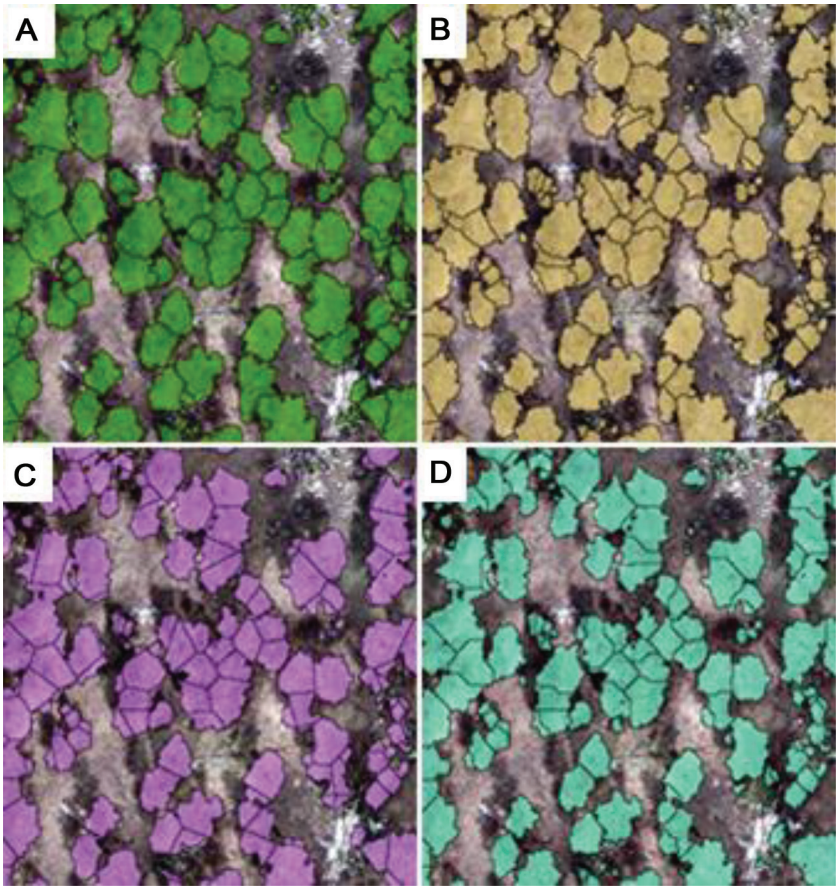

single tree monitoring performance should increase in post-treatment environments for dominant and codominant trees.

Although relative distributions of heights were maintained between observed and detected trees, understory trees experienced higher under-detection rates at MEF compared with KNF (Table 4). The differences in detection accuracy of the understory canopy stratum between the two sites are attributed to the greater density of small trees at MEF, where the stand is experiencing a re-initiation phase with dense regeneration making it difficult to distinguish each individual due to its small size and growing in dense patches. Additionally, previous work has shown spatial clustering of understory trees at MEF (Boyden et al. 2005), likely making it difficult to separate these interlocked crowns and increasing the omission rate. The conical crown shape of most coniferous species make them suitable for the types of tree detection and crown delineation used in this study; however, as crowns become more interlocked or greater proportions of deciduous trees occupy an area, these methods are generally expected to perform worse. This under-detection of understory trees most likely propagates through the crown growing methods, where the crowns of smaller trees are under-segmented, which results in a positive bias in the estimated crown area for smaller trees (Fig. 8). Being able to describe the range of forest environments in which different tree size classes can be reliably detected provides a basis for discussing potential forest management applications.

Applications in forest monitoring

Due to the fine-scale nature of ecological processes within forested ecosystems, capturing variation across tree-to-tree, local neighborhood, and stand-level scales is crucial for understanding forest dynamics. Forest managers of public lands face the challenge of managing for a variety of land uses, and detailed forest structure information with high temporal frequency can aid in spatial forest planning demands. Within open-canopy systems such as ponderosa pine forests, individual tree monitoring through UAS SfM photogrammetry has the potential to provide tree locations and heights with sufficient accuracy and temporal frequency for tracking forest management and disturbance. These tree-level data are a valuable tool in silvicultural prescription development as they enable planning of forest opening and residual groups (Tinkham et al. 2017), as well as facilitating the characterization and monitoring of additional ecological services at a range of spatial scales. For instance, species-specific wildlife habitat, as well as diversity patterns, are often correlated with vertical and horizontal forest structure (Merrick et al. 2013), which can be summarized with tree-level data across landscapes. Additionally, consistent data efficiently acquired through time such as with UAS collections may aid in the monitoring of habitat distributions for species of conservation interest (Vogeler et al. 2016) or for assessing the outcomes of forest restoration activities (Almeida et al. 2019).

Our UAS ITD detection was within 2% and 6% of the number of overstory trees at KNF and MEF, respectively; however, our results reflect the difficulty that ITD methods face when detecting trees in the understory. This high accuracy is promising given the significance of large trees in regulating ecological processes. Larger trees are known to disproportionately impact their surroundings and, in many ecosystems, account for nearly half of all on-site biomass (Hudak et al. 2020). Successful characterization of parameters for large overstory trees is critical for developing mapped estimates of timber volume and aboveground biomass through the application of tree-based allometries (Tinkham et al.

2016*a*). Although RMSE for extracted heights were only 4% at MEF and 10% at KNF, we believe that the true precision of these values is even better as field observations of height typically have −5% bias and 10% precision (Vastaranta et al. 2009).

The tested ITD methods provided reliable detection of overstory and intermediate strata tree locations and heights; however, these methods under-segmented the understory stratum, where small trees in close proximity were identified as a single tree, creating a biased underprediction of small tree densities. Similar under-segmentation has been dealt with through concepts of tree approximate objects to describe ecologically important forest structures in fuels management (Jeronimo et al. 2018). The concept of tree approximate objects suggests that each ITD result may represent a group of trees as each detected tree in the dominant canopy could also represent smaller subordinate trees that are occluded from detection. This more abstract approach still allows for describing the relative variation in forest structure across size classes, which has far-reaching consequences for ecological processes and management prescription development. In planning restoration treatments in pine-dominated forests, the relative density of different tree size classes is important for prescribing the location of openings and retention groups (Addington et al. 2018; Kane et al. 2019). Developing maps that identify areas with dense groups of small trees can help during treatment marking and implementation (Tinkham et al. 2017). Additionally, understanding variation in large tree densities following disturbances such as wildfires could guide reforestation planting efforts (Cannon et al. 2018), as well as facilitate the monitoring of habitat resources for post-fire wildlife species of conservation interest (Vogeler et al. 2016). The approximate observations of tree heights, locations, and crown areas that UAS ITD approaches provide could be a valuable tool for treatment prescription development, marking, and implementation. Furthermore, spatiotemporal data sets of forest structure may contribute to investigations of forest vulnerability to disturbances such as insect outbreaks (Smith et al. 2014).

Most ponderosa pine dominated forests within the central and southern Rocky Mountains with intact disturbance regimes or undergoing restoration have local basal areas of $<$4.6 to 18.4 $m^2 \cdot ha^{-1}$ (Addington et al. 2018). These restored densities are much lower than basal areas seen at the KNF and MEF study areas, giving reason to believe that UAS single tree methods should perform even better across tree sizes when monitoring post-treatment forest conditions. Given the increased potential temporal resolution of UAS monitoring, repeated post-treatment observations could advance our understanding of forest stand and fuel dynamics regarding seedling establishment, seedling and juvenile mortality, and treatment longevity (Tinkham et al. 2016*b*). Further investigation is needed to evaluate these methods for monitoring treated environments and to assess the potential for both identifying new tree recruitment and tracking the growth of individual trees through repeat UAS observations.

Forest monitoring through UAS SfM photogrammetry is still a growing field with further opportunities using multispectral SfM point clouds to unlock other tree characteristics. Recent studies have highlighted the use of multispectral SfM point clouds to classify vegetation (Prošek and Šímová 2019), with similar techniques having the potential to monitor forest health or locate standing dead trees. Coupling ITD and crown growing methods could provide ways of assigning these spectral data to individual trees for deriving a range of additional metrics. Tying this extra information at the individual tree level would enable management prescriptions to target the removal of stressed or sick trees while ensuring retention of snags as critical wildlife habitat. Reliable characterization of tree height, crown area, and the associated spectral signature could provide low-cost and more accessible UAS stand-level observations of forest structure and ecosystem services that cannot be readily captured by traditional field surveys.

Conclusion

This study found that using adaptive variable window ITD methods with UAS-based CHMs increases tree detection rates across tree sizes compared with fixed window methods. The use of UAS SfM-derived high-resolution CHMs allowed for accurate mapping of tree height distributions and tree-level estimation of the crown area. Such characterizations of tree-level forest structure distributions would be valuable for monitoring growth and recruitment dynamics in the face of a changing climate and altered fire and insect disturbance regimes. Further work should explore if the accuracy that we observed for UAS-based ITD methods using variable window functions translates to other forest systems.

Acknowledgements

The authors would like to thank Dr. Mike Battaglia, Dr. Wayne Shepperd, and Lance Asherin for establishing and maintaining these stem-mapped study sites. This project was funded through USDA McIntire-Stennis appropriations to Colorado State University.

References

Addington, R.N., Aplet, G.H., Battaglia, M.A., Briggs, J.S., Brown, P.M., Cheng, A.S., et al. 2018. Principles and practices for the restoration of ponderosa pine and dry mixed-conifer forests of the Colorado Front Range. Gen. Tech. Rep. RMRS-GTR-373, USDA Forest Service, Rocky Mountain Research Station. Fort Collins, Co.

Almeida, D.R.A., Broadbent, E.N., Zambrano, A.M.A., Wilkinson, B.E., Ferreira, M.E., Chazdon, R., et al. 2019. Monitoring the structure of forest restoration plantations with a drone-lidar system. Int. J. Appl. Earth Obs. Geoinform. **79**: 192–198. doi:10.1016/j.jag.2019.03.014.

Andersen, H.-E., Reutebuch, S.E., and McGaughey, R.J. 2006. A rigorous assessment of tree height measurements obtained using airborne Lidar and conventional field methods. Can. J. Rem. Sens. **32**(5): 355–366. doi:10.5589/m06-030.

Belmonte, A., Sankey, T., Biederman, J.A., Bradford, J., Goetz, S.J., Kolb, T., and Woolley, T. 2020. UAV-derived estimates of forest structure to inform ponderosa pine forest restoration. Remote Sens. Ecol. Conserv. **6**(2): 181–197. doi:1. doi:0.1002/rse2.137.

Boyden, S., Binkley, D., and Shepperd, W. 2005. Spatial and temporal patterns in structure, regeneration, and mortality of an old-growth ponderosa pine forest in the Colorado Front Range. For. Ecol. Manage. **219**: 43–55. doi:10.1016/j.foreco.2005.08.041.

Cannon, J.B., Barrett, K.J., Gannon, B.M., Addington, R.N., Battaglia, M.A., Fornwalt, P.J., et al. 2018. Collaborative restoration effects on forest structure in ponderosa pine-dominated forests of Colorado. For. Ecol. Manage. **424**: 191–204. doi:10.1016/j.foreco.2018.04.026.

Cannon, J.B., Tinkham, W.T., DeAngelis, R.K., Hill, E.M., and Battaglia, M.A. 2019. Variability in mixed conifer spatial structure changes understory light environments. Forests, **10**(11): 1015. doi:10.3390/f10111015.

Chave, J., Davies, S.J., Phillips, O.L., Lewis, S.L., Sist, P., Schepaschenko, D., et al. 2019. Ground data are essential for biomass remote sensing missions. Surv. Geophys. **40**: 863–880. doi:10.1007/s10712-019-09528-w.

Churchill, D.J., and Larson, A. 2013. Restoring forest resilience: from reference spatial patterns to silvicultural prescriptions and monitoring. For. Ecol. Manage. **291**: 442–457. doi:10.1016/j.foreco.2012.11.007.

Dalponte, M., and Coomes, D.A. 2016. Tree-centric mapping of forest carbon density from airborne laser scanning and hyperspectral data. Methods Ecol. Evol. **7**(10): 1236–1245. doi:10.1111/2041-210X.12575. PMID:28008347.

Dickinson, Y., Pelz, K.A., Giles, E., and Howie, J. 2016. Have we been successful? Monitoring horizontal forest complexity for forest restoration projects: monitoring horizontal forest complexity. Restor. Ecol. **24**(1): 8–17. doi:10.1111/rec.12291.

Fraser, B.T., and Congalton, R.G. 2018. Issues in Unmanned Aerial Systems (UAS) data collection of complex forest environments. Rem. Sen. **10**: 908. doi:10.3390/rs10060908.

Goodbody, T.R.H., Coops, N.C., Marshall, P.L., Tompalski, P., and Crawford, P. 2017. Unmanned aerial systems for precision forest inventory purposes: a review and case study. For. Chron. **93**(1): 71–81. doi:10.5558/tfc2017-012.

Goutte, C., and Gaussier, E. 2005. A probabilistic interpretation of precision, recall and F-score, with implication for evaluation. *In* Proceedings of the 27th European Conference on Information Retrieval. Springer, Berlin. pp. 345–359. doi:10.1007/978-3-540-31865-1_25.

Heurich, M. 2008. Automatic recognition and measurement of single trees based on data from airborne laser scanning over the richly structured natural forests of the Bavarian Forest National Park. For. Ecol. Manage. **255**(7): 2416–2433. doi:10.1016/j.foreco.2008.01.022.

Hudak, A.T., Fekety, P.A., Kane, V.R., Kennedy, R.W., Filippelli, S.K., Falkowski, M.J., et al. 2020. A carbon monitoring system for mapping regional, annual

aboveground biomass across the northwestern USA. Environ. Res. Lett. **15**(9): 095003. doi:10.1088/1748-9326/ab93f9.

Hummel, S., Hudak, A.T., Uebler, E.H., Falkowski, M.J., and Megown, K.A. 2011. A comparison of accuracy and cost of LiDAR versus stand exam data for landscape management on the Malheur National Forest. J. For. **109**(5): 267–273.

Iglhaut, J., Cabo, C., Puliti, S., Piermattei, L., O'Connor, J., and Rosette, J. 2019. Structure from motion photogrammetry in forestry: a review. Curr. For. Rep. **5**: 155–168. doi:10.1007/s40725-019-00094-3.

Jeronimo, S.M.A., Kane, V., Churchill, D.J., McGaughey, R., and Franklin, J.F. 2018. Applying LiDAR individual tree detection to management of structurally diverse forest landscapes. J. For. **116**(4): 336–346. doi:10.1093/jofore/fvy023.

Kane, V.R., Bartl-Geller, B.N., North, M.P., Kane, J.T., Lydersen, J.M., Jeronimo, S.M.A., et al. 2019. First-entry wildfires can create opening and tree clump patterns characteristic of resilient forests. For. Ecol. Manage. **454**: 117659. doi:10.1016/j.foreco.2019.117659.

Larson, A.J., Stover, K.C., and Keyes, C.R. 2012. Effects of restoration thinning on spatial heterogeneity in mixed-conifer forest. Can. J. For. Res. **42**(8): 1505–1517. doi:10.1139/x2012-100.

Li, W., Guo, Q., Jakubowski, M.K., and Kelly, M. 2012. A new method for segmenting individual trees from the Lidar point cloud. Photogramm. Eng. Remote Sen. **78**(1): 75–84. doi:10.14358/PERS.78.1.75.

Lumley, T. 2020. leaps: Regression subset selection. R package version 3.1 [based on Fortran code by A. Miller]. Available from https://CRAN.R-project.org/package=leaps.

Lutz, J.A. 2015. The evolution of long-term data for forestry: large temperate research plots in an era of global change. Northwest Sci. **89**(3): 255–269. doi:10.3955/046.089.0306.

Lydersen, J.M., North, M.P., Knapp, E.E., and Collins, B.M. 2013. Quantifying spatial patterns of tree groups and gaps in mixed-conifer forests: reference conditions and long-term changes following fire suppression and logging. For. Ecol. Manage. **304**: 370–382. doi:10.1016/j.foreco.2013.05.023.

Martin, K., Aitken, K.E.H., and Wiebe, K.L. 2004. Nest sites and nest webs for cavity-nesting communities in interior British Columbia, Canada: nest characteristics and niche partitioning. Condor, **106**: 5–19. doi:10.1093/condor/106.1.5.

Maturbongs, B., Wings, M.G., Strimbu, B., and Burnett, J. 2019. Forest inventory sensitivity to UAS-based image processing algorithms. Ann. For. Res. **62**(1): 87–108. doi:10.15287/afr.2018.1282.

Merrick, M.J., Koprowski, J.L., and Wilcox, C. 2013. Into the third dimension: benefits of incorporating LiDAR data in wildlife habitat models. *In* Merging Science and Management in a Rapidly Changing World: Biodiversity and Management of the Madrean Archipelago III and 7th Conference on Research and Resource Management in the Southwestern Deserts, 1–5 May 2012, Tucson, Arizona. *Edited by* G.J. Gottfried, P.F. Folliott, B.S. Gebow, L.G. Eskew, and L.C. Collins. USDA Forest Service, Rocky Mountain Research Station, Fort Collins, Colo. Proceedings RMRS-P-67, 67: 389–395.

Mielcarek, M., Stereńczak, K., and Khosravipour, A. 2018. Testing and evaluating different LiDAR-derived canopy height model generation methods for tree height estimation. Int. J. Appl. Earth Obs. Geoinform. **71**: 132–143. doi:10.1016/j.jag.2018.05.002.

Mlambo, R., Woodhouse, I.H., Gerard, F., and Anderson, K. 2017. Structure from Motion (SfM) photogrammetry with drone data: a low cost method for monitoring greenhouse gas emissions from forests in developing countries. Forests, **8**(3): 68. doi:10.3390/f8030068.

Mohan, M., Silva, C., Klauberg, C., Jat, P., Catts, G., Cardil, A., et al. 2017. Individual tree detection from Unmanned Aerial Vehicle (UAV) derived canopy height model in an open canopy mixed conifer forest. Forests, **8**(9): 340. doi:10.3390/f8090340.

Panagiotidis, D., Abdollahnejad, A., Surový, P., and Chiteculo, V. 2017. Determining tree height and crown diameter from high-resolution UAV imagery. Int. J. Rem. Sens. **38**(8-10): 2392–2410. doi:10.1080/01431161.2016.1264028.

Persson, A., Holmgren, J., and Soderman, O. 2002. Detecting and measuring individual trees using an airborne laser scanner. Photo. Eng. Rem. Sens. **68**(9): 925–932.

Plowright, A. 2018. ForestTools: analyzing remotely sensed forest data. R package version 0.2.0. Available from https://CRAN.R-project.org/package=ForestTools

Popescu, S.C., and Wynne, R.H. 2004. Seeing the trees in the forest. Photogramm. Eng. Remote Sens. **70**(5): 589–604. doi:10.14358/PERS.70.5.589.

Prošek, J., and Šímová, P. 2019. UAV for mapping shrubland vegetation: does fusion of spectral and vertical information derived from a single sensor increase the classification accuracy? Int. J. Appl. Earth Obs. Geoinform. **75**: 151–162. doi:10.1016/j.jag.2018.10.009.

R Core Team. 2019. R: a language and environment for statistical computing. R Foundation for Statistical Computing, Vienna, Austria. Available from https://www.R-project.org.

Rhoades, P.R., Davis, T.S., Tinkham, W.T., and Hoffman, C.M. 2018. Effects of seasonality, forest structure, and understory plant richness on bee community assemblage in a southern Rocky Mountain mixed conifer forest. Ann. Entomol. Soc. Am. **111**(5): 278–284. doi:10.1093/aesa/sau021.

Roussel, J.R., Auty, D., Coops, N.C., Tompalski, P., Goodbody, T.R.H., Sánchez Meador, A., Bourdon, J.F., De Boissieu, F., and Achim, A. 2020. lidR: An R package for analysis of Airborne Laser Scanning (ALS) data. Remote Sensing of Environment. **251**: 112061. doi:10.1016/j.rse.2020.112061.

Silva, C.A., Hudak, A.T., Vierling, L.A., Loudermilk, E.L., O'Brien, J.J., Hiers, J.K., et al. 2016. Imputation of individual longleaf pine (*Pinus palustris* Mill.) tree attributes from field and LiDAR data. Can. J. Rem. Sens. **42**(5): 554–573. doi:10.1080/07038992.2016.1196582.

Smith, A.M.S., Kolden, C.A., Tinkham, W.T., Talhelm, A.F., Marshall, J.D., Hudak, A.T., et al. 2014. Remote sensing of vulnerability of vegetation in natural terrestrial ecosystems. Rem. Sens. Environ. **154**: 322–337. doi:10.1016/j.rse.2014.03.038.

Tinkham, W.T., Smith, A.M.S., Hoffman, C.M., Hudak, A.T., Falkowski, M.J., Swanson, M.E., and Gessler, P.E. 2012. Investigating the influence of LiDAR ground surface errors on the utility of derived forest inventories. Can. J. For. Res. **42**(3): 413–422. doi:10.1139/x11-193.

Tinkham, W.T., Smith, A.M.S., Affleck, D.L.R., Saralecos, J.D., Falkowski, M.J., Hoffman, C.M., et al. 2016*a*. Development of height–volume relationships in second growth *Abies grandis* for use with aerial LiDAR. Can. J. Rem. Sens. **42**(5): 400–410. doi:10.1080/07038992.2016.1232587.

Tinkham, W.T., Hoffman, C.M., Ex, S.A., Battaglia, M.A., and Saralecos, J.D. 2016*b*. Ponderosa pine forest restoration treatment longevity: implications of regeneration on fire hazard. Forests, **7**: 137. doi:10.3390/f7070137.

Tinkham, W.T., Dickinson, Y., Hoffman, C.M., Battaglia, M.A., Ex, S., and Underhill, J. 2017. Visualization of heterogeneous forest structures following treatment in the southern Rocky Mountains. Gen. Tech. Rep. RMRS-GTR-365, USDA Forest Service, Rocky Mountain Research Station, Fort Collins, Colo.

Vastaranta, M., Melkas, T., Holopainen, M., Kaartinen, H., Hyyppa, J., and Hyyppa, H. 2009. Laser-based field measurements in tree-level forest data acquisition. Photogramm. J. Finl. **21**(2): 51–61.

Vogeler, J.C., and Cohen, W.B. 2016. A review of the role of active remote sensing and data fusion for characterizing forest in wildlife habitat models. Revista de Teledetección, **45**: 1–14.

Vogeler, J.C., Yang, Z., and Cohen, W.B. 2016. Mapping suitable Lewis's woodpecker nesting habitat in a post-fire landscape. Northwest Sci. **90**(4): 421–432. doi:10.3955/046.090.0404.

Wulder, M.A., White, J.C., Nelson, R.F., Næsset, E., Ørka, H.O., Coops, N.C., et al. 2012. Lidar sampling for large-area forest characterization: a review. Rem. Sens. Environ. **121**: 196–209. doi:10.1016/j.rse.2012.02.001.

Yu, X., Hyyppä, J., Vastaranta, M., Holopainen, M., and Viitala, R. 2011. Predicting individual tree attributes from airborne laser point clouds based on the random forests technique. ISPRS J. Photo. Rem. Sens. **66**(1): 28–37. doi:10.1016/j.isprsjprs.2010.08.003.

Zhen, Z., Quackenbush, L.J., and Zhang, L. 2016. Trends in automatic individual tree crown detection and delineation – evolution of LiDAR Data. Rem. Sens. **8**(4): 333. doi:10.3390/rs8040333.

Ziegler, J., Hoffman, C., Fornwalt, P., Sieg, C., Battaglia, M., Chambers, M., and Iniguez, J. 2017*a*. Tree regeneration spatial patterns in ponderosa pine forests following stand-replacing fire: influence of topography and neighbors. Forests, **8**(10): 391. doi:10.3390/f8100391.

Ziegler, J.P., Hoffman, C., Battaglia, M., and Mell, W. 2017*b*. Spatially explicit measurements of forest structure and fire behavior following restoration treatments in dry forests. For. Ecol. Manage. **386**: 1–12. doi:10.1016/j.foreco.2016.12.002.

Zurqani, H.A., Post, C.J., Mikhailova, E.A., Cope, M.P., Allen, J.S., and Lytle, B.A. 2020. Evaluating the integrity of forested riparian buffers over a large area using LiDAR data and Google Earth Engine. Sci. Rep. **10**(1): 1–16. doi:10.1038/s41598-020-69743-z. PMID:32839474.